

Spatial separation of rotating binary Bose-Einstein condensate by tuning the dipolar interactions*

Ramavarmaraja Kishor Kumar¹, Lauro Tomio^{2,3}, and Arnaldo Gammal¹

¹*Instituto de Física, Universidade de São Paulo, 05508-090 São Paulo, Brazil.*

²*Instituto de Física Teórica, Universidade Estadual Paulista, 01156-970 São Paulo, SP, Brazil.*

³*Instituto Tecnológico de Aeronáutica, DCTA, 12.228-900 São José dos Campos, SP, Brazil.*

(Dated: March 10, 2022)

We are pointing out relevant anisotropic effects, related to spatial separation, miscibility and mass-symmetry, due to dipole-dipole interactions in rotating binary dipolar Bose-Einstein condensates, by considering symmetric (^{164}Dy - ^{162}Dy) and asymmetric (^{168}Er - ^{164}Dy , ^{164}Dy - ^{87}Rb) dipolar mixtures. The binary mixtures are kept in strong pancake-shaped trap, modeled by an effective two-dimensional coupled Gross-Pitaevskii equation. The anisotropy of the dipolar interactions, on miscibility and vortex-lattice structures, is studied by tuning the polarization angle of the dipoles φ , which can enhance the attractive part of the dipole-dipole interaction (DDI) for both inter- and intra-species. Within this procedure of changing to attractive the DDI, a clear spatial separation is verified in the densities at some critical polarization angle. The spatial separations, being angular for symmetric mixtures and radial for asymmetric ones, are verified for repulsive contact interactions when the inter- to intra-species ratio δ is larger than one, implying the system is less miscible. The corresponding result for the critical polarization angle as a function of δ is shown in the particular dipolar symmetric case. A striking outcome of the present study is the observed sensibility of the vortex-pattern binary distributions due to the mass-asymmetry. This is exemplified by the symmetric dipolar mixture, where the two isotopes are of the same species.

I. INTRODUCTION

The realization of Bose-Einstein condensation with chromium (^{52}Cr) atoms has opened the new research direction called dipolar quantum gases [1], allowing first experimental studies on strong dipolar effects in quantum superfluid [2]. Following these investigations with chromium, many subsequent studies have been carried out by different experimental groups on fermionic and bosonic properties of strongly dipolar ultracold gases, such as with dysprosium and erbium [3–10]. Also recently, it was reported in Ref. [11] the realization of two-species mixtures with strongly dipolar atoms, using magneto-optical trap with erbium and dysprosium. By improving the experimental production of dysprosium (^{162}Dy) Bose-Einstein condensates, a new technique was reported in Ref. [12], which allows efficient loading from a magneto-optical trap. Following that, the ability to tune the strength of the dipole-dipole interaction (DDI) has been investigated in Refs. [13, 14], for rotating strongly-dipolar single-atom species. These highly magnetic lanthanide atoms, having strong DDIs, can present quite relevant and interesting quantum behaviors, including ferro-fluidity and self-bound droplets [2, 15, 16]. As demonstrated in Refs. [15], the quantum fluctuations in strongly dipolar Bose gases can stabilize droplets against the mean-field collapse. A recent review considering self-bound droplets can be found in Ref. [17]. Related to vortices in rotating dipolar Bose-Einstein condensates, contrasting with non-dipolar systems, where it is being explored the interplay of magnetism with vorticity,

a review is given in Ref. [18]. Novel fascinating possibilities in physics are being revealed by the researchers with strongly dipolar binary mixtures [11], due to the peculiar competition between isotropic short-range contact interaction and long-range anisotropic DDI. Apart from experimental studies, there are previous investigations on the stability of trapped dipolar Bose-Einstein condensates in Ref. [19], as well as several theoretical studies performed with dipolar mean-field theory, which are based on the construction of the corresponding pseudo-potential [20, 21]. Following that, on binary dipolar mixtures, one can also find out more recent theoretical investigations as, for example, in Ref. [22], where it was studied the effect of a second dipolar BEC on the stability properties of binary dipolar mixtures in pancake-trapped symmetry. The ferrofluid-like pattern formations are studied in two-component BEC with DDI in Ref. [23], with instabilities and pattern formations (verified by oppositely polarized dipoles in a two-component BEC) being recently reported in Ref. [24]. Rotational properties of two-component dipolar BEC in concentrically coupled annular traps were also studied in Ref. [25], by assuming one component without dipole moments. The immiscibility-miscibility transition of a two-component dipolar BECs, previously studied in Ref. [26], was further investigated by some of us in Ref. [27], where it was determined the miscibility properties of binary mixtures with the isotopes $^{162,164}\text{Dy}$ and ^{168}Er within a three-dimensional (3D) formalism. When considering the miscibility, it was also shown in Ref. [28] that the rotational properties of symmetric and asymmetric dipolar mixtures present quite distinct vortex lattice structures.

In the present work we investigate properties of strong dipolar mixtures in a two-dimensional (2D) rotating mag-

* Corresponding author: tomio@ift.unesp.br

netic trap, by tuning the dipole-dipole interaction, adjusting the polarization angle between dipoles, within a coupled Gross-Pitaevskii (GP) formalism. In view of previous stability analysis and analytical considerations on miscibility and expected vortex-pattern structures, our approach is fully performed by exact numerical solutions of the corresponding formalism. These studies are motivated by the recent improvements in the experimental techniques [11], in order to control the dipole orientations of dipolar condensed atoms and explore new physics. By tuning the dipoles larger than the angle aligned along the z -axis provides an attractive component in the DDI. Since, the self-bound droplets require a balance between repulsive and attractive interactions, by controlling the dipole orientations it is expected to reach more favorable conditions for the observation of self-bound droplets. The stability of dipolar BECs affected by the attractive part of the DDI can be kept by using strong axially confining pancake-shaped trap, with suitable repulsive contact interactions. Therefore, within a study which can be easily extended to other binary mixtures, we consider in particular atomic species having strong magnetic dipolar properties, such as the ones used in the recent BEC experiments reported in Refs. [7, 11]. So, our main focus are the binary mixtures having the isotopes of dysprosium $^{162,164}\text{Dy}$ and erbium ^{168}Er . For comparison, in our analysis we also include a binary mixture in which one of the species is the weakly dipolar rubidium ^{87}Rb .

We assume a configuration in which the dipoles are oriented along the z -axis, within a quasi-2D settings where the dipoles are parallel to each other in the (x, y) -plane. By tuning the dipoles, exploring anisotropic effects due to DDI in the (x, y) -plane, different properties are evidenced for the rotating binary mixtures. Using this procedure to alter the DDI from repulsive to attractive, one can further explore condensate properties of coupled systems for different contact interactions. Some of the relevant properties of the strong dipolar binary systems considered in this work (^{164}Dy - ^{162}Dy , ^{168}Er - ^{164}Dy , and ^{164}Dy - ^{87}Rb), have been studied recently. In Ref. [27], within a full 3D formalism, it was established the miscible-immiscible stable conditions of these coupled dipolar systems with repulsive contact interactions, from pancake-to cigar-type trap configurations. The rotational properties and vortex-lattice structures were further investigated in Refs. [28, 29]. More recently, in Ref. [30], we have also investigated the effect of changing the inter-to intra-species scattering length in these strong dipolar systems under squared optical lattices. These mentioned works helped us to better define some characteristics of such dipolar binary systems which can be relevant for experimental realization. Among these characteristics, one should noticed the possibility of tuning the polarization angles of both interacting dipoles, such that the effective time-averaged dipole-dipole potential can be modified from repulsive to attractive interactions. Therefore, it is expected that the interplay between DDIs and contact interactions can bring us some possible inter-

esting effect in the rotational properties of binary dipolar systems. Within such motivation, by considering the above strongly dipolar binary systems kept in quasi-2D pancake-shaped traps, our main task is to investigate possible anisotropic effects due to dipole-dipole interactions in rotating binary dipolar Bose-Einstein condensates. In this case, by assuming fixed the rotation frequency and trap aspect ratio, we have two independent mechanisms to control the inter- and intra-species interactions: Feshbach resonance techniques [31], controlling the contact interactions; and the tuning of the polarization angle, modifying the dipole-dipole interactions.

By considering the interplay between the contact and dipolar interactions, some peculiar non-trivial behaviors emerge in the density distributions, which for symmetric mixtures such as ^{164}Dy - ^{162}Dy are quite distinct than the corresponding distributions for non-symmetric ones as ^{168}Er - ^{164}Dy , and ^{164}Dy - ^{87}Rb . Symmetric dipolar mixtures with isotopes of the same atomic species are quite interesting to study due to the rich variety of patterns that one can create in the density distributions, from geometric vortex structures to droplet-like formations. Interesting enough, it also leads to an almost complete half-space angular separation between the species, for some critical polarization angle when the DDI is attractive. The observation of a critical polarization angle, at which an almost complete spatial separation occurs between the two densities when the DDI is attractive, is quite remarkable for both symmetric and asymmetric mixtures. Being half-space angular for the dipolar symmetric mixture, the spatial separation of the densities turns out to be radial in case of asymmetric mixtures. Beyond that, the particular case of dipolar-symmetric mixture provides us the opportunity to verify the effect of mass-symmetry breaking in the two-component vortex-pattern structures. When considering a small change in the mass, the sensitivity of the patterns is evidenced with a fixed rotation parameter and by adjusting to the same value the inter- and intra-species contact interactions.

Next, we present the basic formalism and notation, followed by a section with our main results for the three kind of dipolar mixtures we consider. In a final section, we have a summary with our main conclusions.

II. FORMALISM AND PARAMETRIZATION

The coupled dipolar system with condensed two atomic species are assumed to be confined in strongly pancake-shaped harmonic traps, with fixed aspect ratios, such that $\lambda = \omega_{i,z}/\omega_{i,\perp} = 20$ for both species $i = 1, 2$, where $\omega_{i,z}$ and $\omega_{i,\perp}$ are, respectively, the longitudinal and transverse trap frequencies. The coupled Gross-Pitaevskii (GP) equation is cast in a dimensionless format by measuring the energy in units of $\hbar\omega_{1,\perp}$, with the length in units of $l_{\perp} \equiv \sqrt{\hbar/(m_1\omega_{1,\perp})}$, where $\omega_{1,\perp} \equiv \omega_1$ and m_1 are the transverse frequency and mass for the species $i = 1$. Correspondingly, the space and time variables are given in units of l_{\perp} and $1/\omega_1$, respectively, such that $\mathbf{r} \rightarrow l_{\perp}\mathbf{r}$

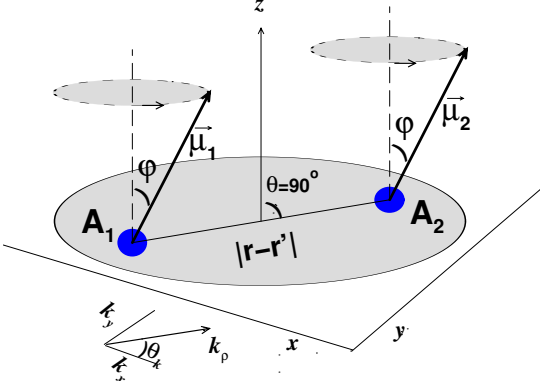


FIG. 1. An illustration of the DDI between the two atomic species 1 and 2, given in coordinate space, where the polarization angle is φ , with the assumption that both atoms are in the (x, y) plane ($\theta = 90^\circ$).

and $t \rightarrow \tau/\omega_1$). Within these units, and by adjusting both trap frequencies such that $m_2\omega_{2,\perp}^2 = m_1\omega_{1,\perp}^2$, the dimensionless external three-dimensional (3D) trap potential for both species can be written as

$$V_{3D}(\mathbf{r}) = \frac{1}{2}(x^2 + y^2 + \lambda^2 z^2) \equiv V(x, y) + \frac{1}{2}\lambda^2 z^2. \quad (1)$$

In the case of the DDI, we consider that one of the atoms (A_i) is at position \mathbf{r} , with the other one (A_j) at position \mathbf{r}' , respectively, with their line-vector $\mathbf{r} - \mathbf{r}'$ making an angle θ related to the z -axis, such that $\theta \approx 90^\circ$ for a strong pancake-shaped trap as given by Eq. (1) (each one of the atoms can be of species $i, j = 1, 2$). Next, we assume both dipoles are polarized in the same direction, making an angle φ with respect to the z -axis. See the corresponding illustration in the Fig. 1. The tunability is performed by using time-dependent magnetic fields with dipoles rapidly rotating around the z -axis [32, 33]. The magnetic field is given by the combination of a static part along the z -direction and a fast rotating part in the (x, y) -plane, having a frequency such that the atoms are not significantly moving during each period. Once performed a time averaging of the DDI within a period, the corresponding 3D averaged interaction between the coupled dipolar species i and j , with their respective magnetic dipole moments μ_i and μ_j given in terms of the Bohr magneton μ_B , can be written in our dimensionless format as [33]

$$\langle V_{3D}^{(d)}(\mathbf{r} - \mathbf{r}') \rangle_{ij} = \frac{\mu_0 \mu_i \mu_j}{\hbar \omega_1 l_\perp^3} \frac{1 - 3 \cos^2 \theta}{|\mathbf{r} - \mathbf{r}'|^3} \left(\frac{3 \cos^2 \varphi - 1}{2} \right), \quad (2)$$

where μ_0 is the free-space permeability. In the following, we assume $\theta = 90^\circ$, such that the DDI strength is repulsive for $\varphi < \varphi_M$ and attractive when $\varphi > \varphi_M$ (where $\varphi_M \approx 54.7^\circ$ is the so-called “magic angle”, when the DDI is averaged to zero). The factor within parenthesis in Eq. (2) results from the time-averaging procedure on the dipole orientation around the z -axis. A large value for the aspect ratio λ allows us to reduce the original 3D formalism to a 2D, by considering the

usual factorization of the 3D wave function into the 2D wave function $\psi_i(x, y, \tau)$ and the ground state of the transverse harmonic oscillator trap, given by the ansatz $(\lambda/\pi)^{1/4} e^{-\lambda z^2/2}$. The two-body contact interactions related to the scattering lengths a_{ij} , as well as the dipole-dipole interaction parameters for the species $i, j = 1, 2$, are defined as [27]

$$g_{ij} \equiv \sqrt{2\pi\lambda} \frac{(m_1 + m_2)}{m_2} \frac{a_{ij} N_j}{l_\perp}, \quad d_{ij} = \frac{N_i}{4\pi} \frac{\mu_0 \mu_i \mu_j}{\hbar \omega_1 l_\perp^3},$$

$$a_{ii}^{(d)} \equiv \frac{1}{12\pi} \frac{m_i}{m_1} \frac{\mu_0 \mu_i^2}{\hbar \omega_1 l_\perp^2}, \quad a_{12}^{(d)} = a_{21}^{(d)} = \frac{1}{12\pi} \frac{\mu_0 \mu_1 \mu_2}{\hbar \omega_1 l_\perp^2}, \quad (3)$$

where $N_{j=1,2}$ is the number of atoms of the species j . In the next, the length unit will be adjusted to $l_\perp = 1 \mu\text{m} \approx 1.89 \times 10^4 a_0$, where a_0 is the Bohr radius, such that a_{ij} and $a_{ij}^{(d)}$ can be conveniently given in terms of a_0 in our numerical analysis.

With the above notations for units and parameters, the corresponding coupled GP equation in 2D is given by

$$i \frac{\partial \psi_i}{\partial \tau} = \left[\frac{-m_1}{2m_i} \left(\frac{\partial^2}{\partial x^2} + \frac{\partial^2}{\partial y^2} \right) + V(x, y) - \Omega L_z + \sum_{j=1,2} g_{ij} |\psi_j|^2 \right. \\ \left. + \sum_{j=1,2} d_{ij} \int_{-\infty}^{\infty} dx' dy' V^{(d)}(x - x', y - y') |\psi_j'|^2 \right] \psi_i, \quad (4)$$

where $V^{(d)}(x, y)$ is the reduced 2D expression for the DDI, and $\psi_i \equiv \psi_i(x, y, \tau)$ and $\psi_i' \equiv \psi_i(x', y', \tau)$ are the components of the total 2D wave function, normalized to one, $\int_{-\infty}^{\infty} dx dy |\psi_i|^2 = 1$. L_z is the angular momentum operator with Ω the corresponding rotation parameter (in units of ω_1), which is common for the two components. The external potential provided by the harmonic trap is given by $V(x, y) = \frac{1}{2}(x^2 + y^2)$.

In 2D momentum space, the DDI can be expressed as the combination of two terms, considering the orientations of the dipoles φ and projection of the Fourier transformed of $V^{(d)}(x, y)$ in momentum space; one term perpendicular with the other parallel to the direction of the dipole inclinations, respectively given by [26, 29]

$$\tilde{V}_\perp^{(d)}(k_x, k_y) = 2 - 3 \sqrt{\frac{\pi}{2\lambda}} k_\rho \exp\left(\frac{k_\rho^2}{2\lambda}\right) \text{erfc}\left(\frac{k_\rho}{\sqrt{2\lambda}}\right), \quad (5)$$

$$\tilde{V}_\parallel^{(d)}(k_x, k_y) = -1 + 3 \frac{k_x^2}{k_\rho} \sqrt{\frac{\pi}{2\lambda}} \exp\left(\frac{k_\rho^2}{2\lambda}\right) \text{erfc}\left(\frac{k_\rho}{\sqrt{2\lambda}}\right), \quad (6)$$

where $k_\rho^2 \equiv k_x^2 + k_y^2$, with $\text{erfc}(x)$ being the complementary error function of x . The k_x explicit in the right-hand-side of the above parallel term is the projected wave-number in the (x, y) plane, in the direction of the polarization tilt, which was arbitrarily assumed in the x -axis when derived that term [26]. Generalizing the description to a polarization field rotating in the (x, y) plane, as $\mathbf{k}_\rho = (k_x, k_y) = (k_\rho \cos \theta_k, k_\rho \sin \theta_k)$ and all directions θ_k are equally possible, we should average $k_\rho^2 \cos^2 \theta_k$ in the plane, such that k_x^2 should be replaced by $k_\rho^2/2$ in the parallel term shown in Eq. (6). Therefore, by combining the two terms according to the orientations φ of the dipoles, we obtain the total 2D momentum-space DDI, $\tilde{V}^{(d)}(k_x, k_y) =$

$\cos^2(\varphi)\tilde{V}_\perp^{(d)}(k_x, k_y) + \sin^2(\varphi)\tilde{V}_\parallel^{(d)}(k_x, k_y)$, which can be written as

$$\tilde{V}^{(d)}(k_x, k_y) = \frac{3\cos^2(\varphi) - 1}{2}\tilde{V}_\perp^{(d)}(k_x, k_y) \equiv V_\varphi(k_\rho). \quad (7)$$

It follows that the effective DDI in 2D configuration space shown in Eq. (4) is obtained by applying the convolution theorem, performing the inverse 2D Fourier-transform for the product of the DDI and density, such that $\int dx'dy' V^{(d)}(x - x', y - y') |\psi'_j|^2 = \mathcal{F}_{2D}^{-1} [\tilde{V}^{(d)}(k_x, k_y) \tilde{n}_j(k_x, k_y)]$. From Eqs. (5) and (7), one should noticed that such momentum-space Fourier transform of the dipole-dipole potential is changing the signal at some particular large momentum k_ρ . However, after applying convolution theorem with the inverse Fourier transform (by integrating the momentum variables), the corresponding coordinate-space interaction has a definite value, as in the 3D case, which is positive for $\varphi \leq \varphi_M$, and negative for $90^\circ \geq \varphi > \varphi_M$. For larger angles, when the DDI is predominantly attractive, close to $\varphi \approx 90^\circ$, the system can become unstable, requiring enough repulsive contact interactions and suitable strong pancake-shaped trap. In view of these requirements, in order to stabilize the binary dipolar rotating system also in this extreme dipolar condition, along this work we have assumed a quite strong aspect ratio $\lambda = 20$ for the trap, with the intra-species contact interactions ($a_{ii} = 50a_0$) enough large and equal for both atomic elements.

In the next subsection, we provide more details on the specific parametrization and numerical approach considered in our study.

A. Parameters and numerical approach

The magnetic dipole moments of the considered dipolar atoms given in terms of the Bohr magneton μ_B , are the following: $\mu = 10\mu_B$ for $^{162,164}\text{Dy}$, $\mu = 7\mu_B$ for ^{168}Er , and $\mu = 1\mu_B$ for ^{87}Rb . In particular, considering the corresponding dipole moments, the strengths of the DDI are given as $a_{ij}^{(d)} = 131a_0$ ($i, j = 1, 2$), for the ^{164}Dy - ^{162}Dy mixture; and $a_{11}^{(d)} = 66a_0$, $a_{22}^{(d)} = 131a_0$ and $a_{12}^{(d)} = a_{21}^{(d)} = 94a_0$, for the ^{168}Er - ^{164}Dy mixture. As the magnetic moment of ^{87}Rb is negligible in comparison with the ^{164}Dy , we assume the binary mixture ^{164}Dy - ^{87}Rb as being single-species dipolar, such that $a_{22}^{(d)} = a_{12}^{(d)} \approx 0$. To explore the anisotropic effect of the DDI, we vary the polarization angle φ , which influence the inter-, and intra-species dipolar interactions. Initially the dipoles are considered to be polarized along the z -axis with the polarization angle $\varphi = 0^\circ$, which provides repulsive DDI. Since, we do not have a separate control to tune the inter-species dipolar interaction, tuning the polarization angle of dipoles $\varphi > 0$ starts to provide attractive dipolar interaction in all the components of inter- and intra-species dipolar interaction. Apart from dipolar parameters, other intrinsic properties

of binary systems are related to the two-body contact interactions, which in principle can be varied by using Feshbach techniques [31]. By keeping our study in stable systems, all the two-body scattering lengths are assumed to be positive, with the intra-species ones being identical and given by $a_{11} = a_{22} = 50a_0$ (a_0 is the Bohr radius), with the inter-species one, a_{12} , obtained from the ratio $\delta = a_{12}/a_{11}$. Relevant for the vortex-patterns that we are studying, we allow δ to be changed in a region of interest in the parameter space, from smaller to larger values. The δ is considered as follows, for the miscible mixture $\delta = 0.75$, intermediate level where one may find partially miscible at $\delta = 1.0$ and for completely immiscible mixtures $\delta = 1.1, 1.25$ and 1.45 . The rotation frequency smaller than $\Omega < 0.4$ may not enough to observe vortex lattice structures. From the previous study and numerical test, we choose the rotation frequency $\Omega = 0.6$, which is enough to produce the vortex lattice structures within the parameters that we considered in the present study. For the harmonic trap potential, a strong pancake-shaped trap in the (x, y) -plane is applied, with an aspect ratio $\lambda = 20$, with the atom numbers fixed for both species at $N_1 = N_2 = 10^4$. These choices are appropriate for experimental realistic settings due to stability requirements. Once defined the transversal trap frequency for the first species as given by $\omega_1 = 2\pi \times 60\text{s}^{-1}$, the trap frequencies for the second species can be found from our assumption on the angular frequencies such that $m_2\omega_2^2 \simeq m_1\omega_1^2$, implying that the trap frequencies are about the same for both species in the cases of ^{164}Dy - ^{162}Dy and ^{168}Er - ^{164}Dy binary mixtures; whereas for the ^{164}Dy - ^{87}Rb the trap frequency of the rubidium is $\omega_2 \approx 2\pi \times 82\text{s}^{-1}$.

In our analysis of coupled binary mixtures, a relevant property that affects strongly the vortex patterns is the miscibility of the system, which varies according to the inter- and intra-species interactions (contact and/or dipolar in the present case). In order to estimate that, we use a parameter defined and studied in Ref. [27], given by

$$\eta \equiv \int |\psi_1| |\psi_2| dx dy, \quad (8)$$

implying in $\eta = 1$ for a complete miscible system, with $\eta = 0$ for a complete immiscible one.

Related to the numerical procedure to solve Eq. (4), as in Ref. [27], we apply the split-step Crank-Nicolson method [34, 35], combined with a standard method for evaluating DDI integrals in the momentum space (see details in Ref. [28] and references therein). In order to search for stable solutions, in the present work the numerical simulations were carried out in imaginary time on a grid with a maximum of 528 points in each x and y directions x and y , with spatial and time steps $\Delta x = \Delta y = 0.05$ and $\Delta t = 0.0005$, respectively. Both component wave functions are renormalized to one at each time step. In order to obtain stationary vortex states, we solve the Eq. (4) with different initial conditions. In view of previous tests on the initial suitable

conditions, we use combination of angular harmonics followed by convergence tests of the solutions for the given inputs, within a procedure also discussed in Ref. [28].

III. RESULTS ON BINARY DIPOLAR MIXTURES

Our main results are presented in this section, which are verified by tuning the DDI from repulsive to attractive, leading to an almost complete spatial phase separation of rotating binary mixtures at some critical orientation of the dipoles, when the DDI becomes attractive. We consider three dipolar coupled BEC mixtures, which have different natural characteristics in respect to their miscibility properties, as well as different vortex-pattern structures when the binary system is under rotation, as verified in previous studies [27, 28]. First, we consider a symmetric-dipolar coupled system, ^{164}Dy - ^{162}Dy , where both magnetic dipoles have the same value, which is more miscible when both species have the same polarization, $\varphi = 0$. Next, we consider an asymmetric-dipolar mixture, the ^{168}Er - ^{164}Dy , which is less miscible, having both species with large but different magnetic dipoles. Finally, in order to compare with the previous two cases, we also examine the ^{164}Dy - ^{87}Rb case, considering it as a single-dipolar binary mixture, as one of the species have negligible dipole moment.

In all the cases that we are presenting, as explained in the previous section, some of the parameters are fixed to approximate realistic values considered in experiments, as well as fixed by favorable stability conditions. With the parameters as number of atoms for each species, trap aspect ratio, intra-species scattering lengths and rotation frequency settled, our study is concentrated in the main focus of our work, which is to explore the behavior of a strong dipolar coupled system, by tuning the polarization angle of the dipoles (varied from zero to 90°) together with variations of the inter- to intra-species two-body contact interactions δ . In view of the miscibility properties of the binary dipolar mixtures, the parameter δ determines the initial vortex patterns (when $\varphi = 0$ and the DDI is repulsive). By increasing φ , the DDI can be modified to be attractive, which happens for $\varphi > 54.7^\circ$.

A. The symmetric-dipolar ^{164}Dy - ^{162}Dy binary mixture

Within our aim to analyze the anisotropic property of the dipolar interactions by tuning the dipoles from $\varphi = 0^\circ$ to 90° , we first consider the nearly symmetric mixture ^{164}Dy - ^{162}Dy , where both dipolar species have the same magnetic dipole moments, with the coupled system being more miscible than the other two cases we are studying; at least when the DDI is repulsive. As verified in Ref. [28], this dipolar mixture can show triangular, squared, striped, and domain wall vortex-

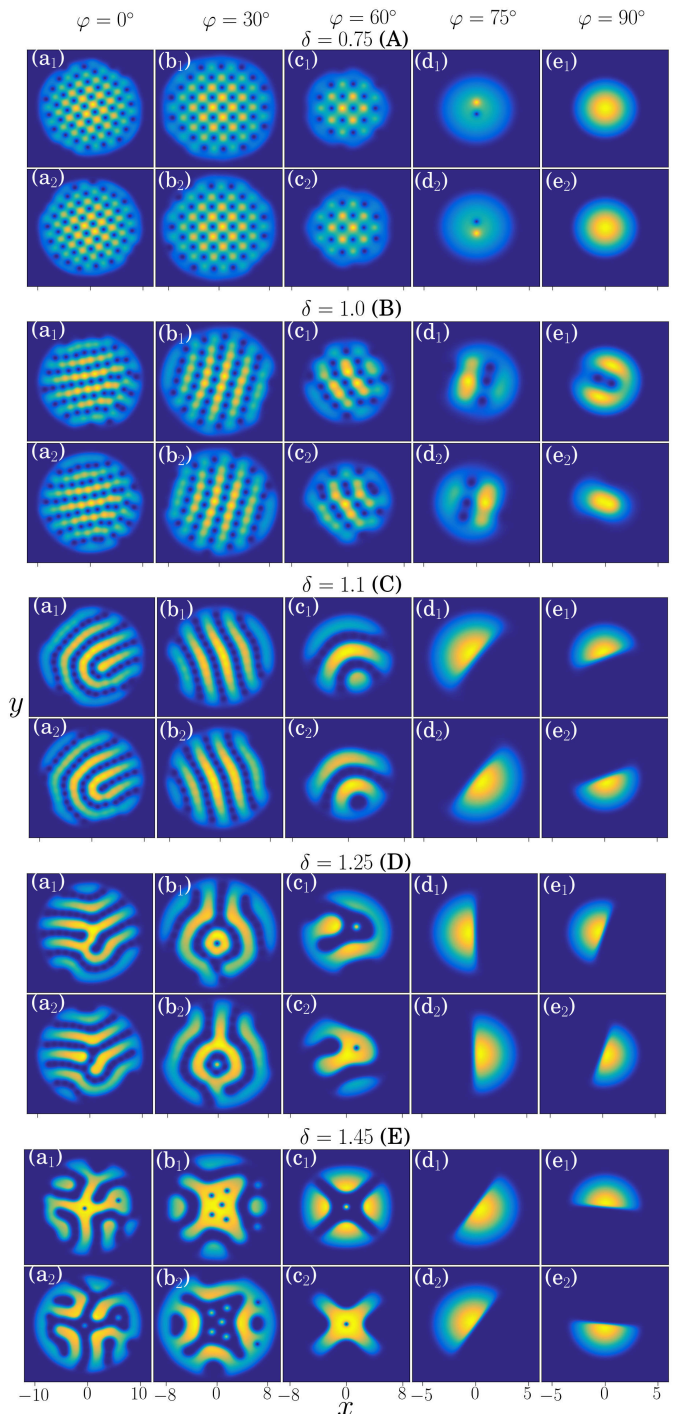


FIG. 2. (Color on line) The 2D densities $|\psi_{j=1,2}|^2$ are shown for the ^{164}Dy - ^{162}Dy dipolar mixture ($j = 1$ is the ^{164}Dy , with $j = 2$ the ^{162}Dy), by tuning the polarization φ from 0° [(a_j)] to 90° [(e_j)], with δ varying from 0.75 [set (A)] to 1.45 [set (E)]. All panels have square (x, y) dimensions, indicated by the x -labels. The (x, y) are dimensionless, with $l_\perp = 1\mu\text{m}$ being the space unit. The density levels vary from 0 (darker) to a limit ranging $0.009 \sim 0.12$ (lighter), fixed by their respective normalization to one.

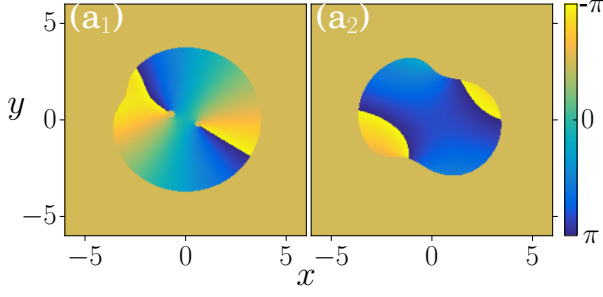


FIG. 3. (Color on line) Phase diagrams ($a_{j=1,2}$) for the densities $|\psi_j|^2$ of the double-core vortices, corresponding to panels (e_j) of Fig. 2(B), when the DDI is purely attractive ($\varphi = 90^\circ$). The (x, y) and $|\psi_j|^2$ are dimensionless, with $l_\perp = 1\mu\text{m}$ being the space unit.

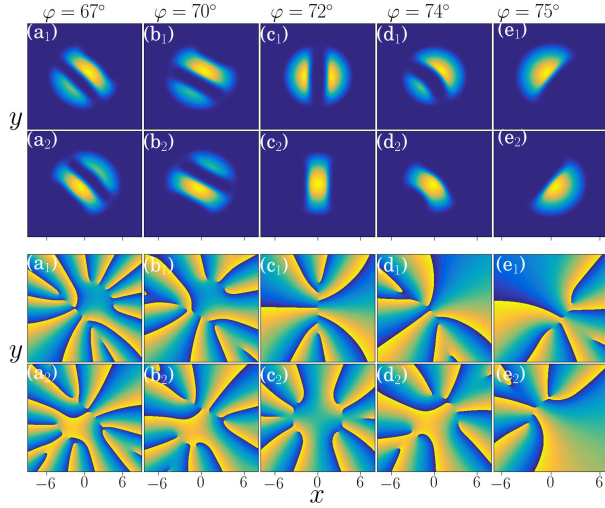


FIG. 4. (Color on line) 2D densities $|\psi_{j=1,2}|^2$ are shown in the upper two sequence of panels, for the ^{164}Dy - ^{162}Dy mixture, as in Fig. 2(C) ($\delta = 1.1$), but considering the tuning-polarization angle from 67° [(a_j)] to 75° [(e_j)]. The corresponding phase diagrams, using the same respective labels (a_j) for 67° to (e_j) for 75° , are given in the lower two sequence of panels, with hidden vortices being confirmed. The (x, y) and $|\psi_j|^2$ are dimensionless, with $l_\perp = 1\mu\text{m}$ being the space unit.

lattice structures regarding to the ratio between inter- and intra-species contact interaction δ and rotation frequency Ω . The rotation in the present study is fixed to $0.6\omega_\perp$, guided from a previous study in Ref. [28], as found it is appropriate (not too large or small) to study other properties of binary dipolar systems trapped in 2D pancake-type geometries, such as the behaviors due to changes in the contact and dipolar interactions. In the absence of contact interaction, the inter-, and intra-species dipolar interactions are balanced and behaves like the case having $\delta = 1$. So, the main characteristics of this dipolar symmetric system is that, being more miscible it is expected to present striped-vortex patterns as δ

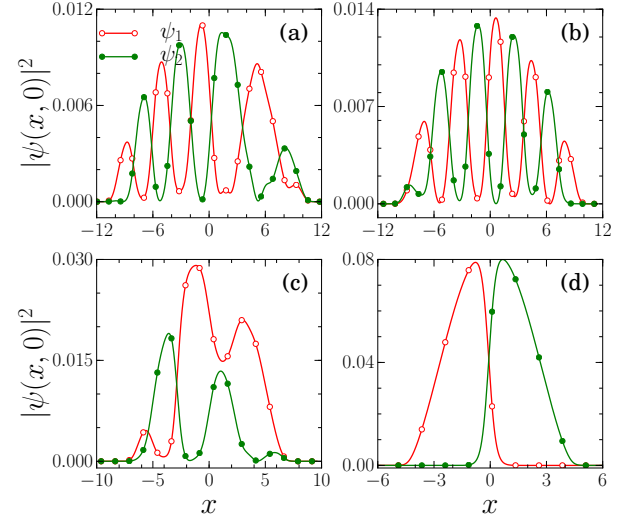


FIG. 5. (Color on line) Densities, given in 1D for $y = 0$, are shown for the binary mixture ^{164}Dy - ^{162}Dy , corresponding to $\delta = 1.1$, Fig. 2(C), for the polarization angles $\varphi = 0^\circ$ (a), 30° (b), 60° (c), and 75° (d). In particular, the panel (d) shows the mixture reaching an almost-complete spatial separation of the densities. The (x, y) and $|\psi_j|^2$ are dimensionless, with $l_\perp = 1\mu\text{m}$ being the space unit.

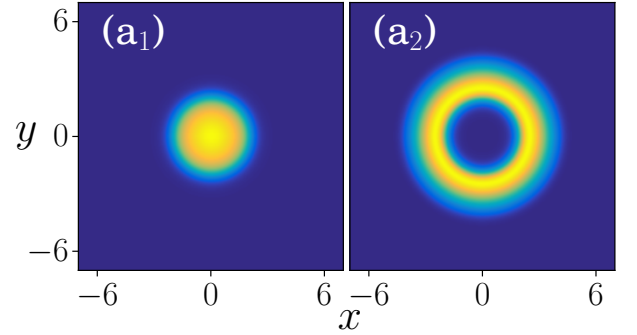


FIG. 6. (Color on line) Nonrotating ($\Omega = 0$) condensate densities for the dipolar mixture ^{164}Dy - ^{162}Dy , considering $\delta = 1.1$ and $\varphi = 75^\circ$, corresponding to panels (d_j) of Fig. 2(C). The (x, y) and densities are dimensionless, with $l_\perp = 1\mu\text{m}$ being the space unit.

is increased, when the dipoles are both polarized in the same direction, which are clearly verified in the panels (a_j) of Fig. 2(B). The density patterns change quite significantly by increasing δ , particularly when the coupled system becomes attractive.

From the results shown in Fig. 2, where we have a few specific sets for fixed values of δ from 0.75 till 1.45, one can extract some general characteristics. First we notice that the sizes of the condensates (each species $j = 1, 2$) remain approximately the same as we increase δ , for some given polarization angle φ . As, in this case, the dipolar

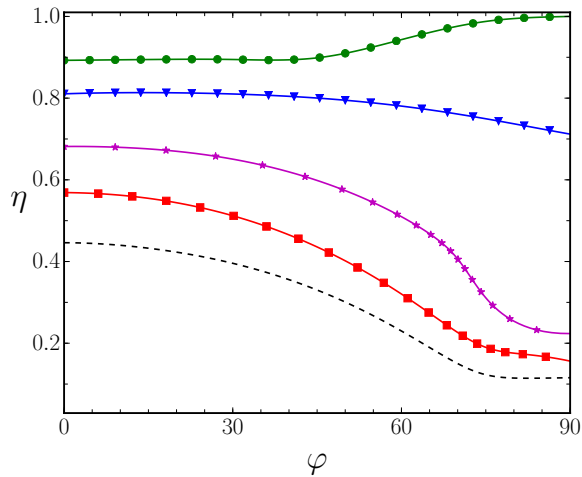


FIG. 7. (Color on line) The miscibility parameter (η), defined in Eq. (8), is shown as function of the polarization angle φ , for the five cases of inter- to intra-species contact interactions presented in Fig. 2. For $\delta = 0.75$, we have the green-solid line with circles; for $\delta = 1.0$, the blue-solid line with triangles; for $\delta = 1.1$, the purple-solid line with stars; for $\delta = 1.25$, the red-solid line with squares; and for $\delta = 1.45$ the dashed line.

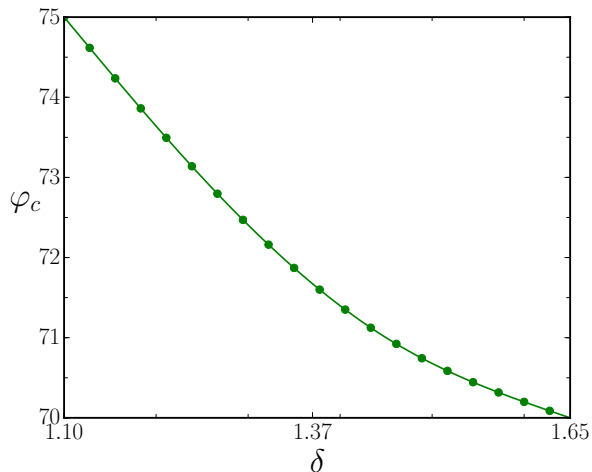


FIG. 8. Critical angle φ_c for the almost-complete spatial separation of the mixture ^{164}Dy - ^{162}Dy , considering the relevant interval region of δ that we are studying.

parameters are also fixed, together with the intra-species contact interactions ($a_{jj} = 50a_0$), we are verifying that the relevant role of the inter-species contact interaction ($a_{12} = a_{jj}\delta$) is mainly in the vortex-pattern structures and miscibility, with practically no interference on the sizes of the condensates. Only for fixed angles $\varphi \geq 75^\circ$ (when the DDI is more attractive) we observe some small effect of δ in the radius, which slightly increase for larger values of δ ; an effect which will be clarified as due to the formation of vortices in the coupled system as $\delta \geq 1$, resulting in some extra repulsive internal forces opposing

the attractive DDI.

For the DDI, we should first observe that the polarization angle φ is the only parameter affecting both inter- and intra-species dipole interactions in the same way. However, as already observed in the case of contact interactions, the main responsible for the sizes of the density distributions are the intra-species forces. As the corresponding contact interactions are kept fixed, the sizes of the density distributions are reduced by increasing the attractive DDI, φ approaching 90° . The condensates shrink due to more intra-species dipolar attraction. The DDI is averaging exactly to zero at the particular case for $\varphi = \varphi_M = 54.7^\circ$, where φ_M is the so-called “magic-angle”. So, at this angle, no effect is expected from the DDI, such that the observed vortex-pattern structures should only due to the rotation angle, contact interactions and corresponding mass differences of the coupled mixtures.

The most striking result we found in this symmetric-dipolar case occurs due to the mass-symmetry breaking, represented by the set with $\delta = 1$, in Fig. 2(C). By considering $m_2 = m_1$ in Eqs. (4) and (3), the coupled two-component equation reduces to a single-component one, implying that the results presented in the upper and lower panels of Fig. 2(C) should be identical. This is confirmed by our numerical approach in solving the coupled system Eq. (4). We should noticed that, the mass asymmetry we have in this case, $\delta_M = 1/81$, is quite small and appears only in two terms of the dimensionless Eq. (4). The results shown in Fig. 2, by considering a fixed $\delta > 1$, are reflecting the relevant changes in the vortex patterns when we increase this polarization angle near φ_M (from 30° , when it is repulsive, to 60° , when it is attractive). By decreasing the repulsion of the dipoles, the vortices merge together providing striped structures in the coupled densities, which happen because the coupled system is less miscible when the inter-species is larger than the intra-species interaction ($\delta > 1$).

In an analysis provided in Ref. [36], when considering that the only nonlinear repulsive forces in a rotating coupled system are due to contact interactions, the structure and boundary domains of stripes are discussed by using an approximate Thomas-Fermi profile. However, the analysis was restricted to the symmetric case with $\delta = 1$, when all the masses and frequencies and number of atoms are identical for both species. This is further verified in the same reference that is quite approximate for $\delta > 1$. In the present case, the corresponding behavior can be directly followed from results shown in Fig. 2, by considering in particular the columns (a_i) to (c_i), for fixed repulsive DDI, when $\varphi \lesssim 60^\circ$. As shown, the stripes become larger by increasing the inter-species interaction δ , changing to serpentine-like and domain-wall patterns. This implies that to estimate how the boundaries of the stripe increase one cannot rely in an approximation in which there is no asymmetry in the contact interactions (when all the other parameters for the species are identical), as this will correspond to a single-species interac-

tion.

Correspondingly, one could try to extend the analysis performed in Ref. [36] to the cases that we have δ fixed, changing the DDI by tuning the angle φ . As shown in Fig. 2(C), for example, the stripes are becoming wider when the DDI is more attractive; presenting a behavior not similar as the observed for the contact interactions. The problem is that both dipolar and contact interactions are not being varied in the same way. When we vary the DDI by tuning the dipoles, all the inter- and intra-species are being changed in the same way, such that the ratio between inter- and intra-species dipolar interaction remains fixed, whereas when changing δ only the inter-species interactions are being modified. So, for the DDI, the dominant behavior which is being verified is due to the increasing intra-species dipolar attraction when moving φ to larger angles. The condensates start to shrink, reducing the space of the overlap between the two species. From one side, by increasing δ , as shown before the binary system becomes less miscible; and from the other side, the coupled condensate are shrinking by increasing the DDI. Together, the interplay of these two effects will result in an almost complete space separation between the densities, as observed in Fig. 2 for $\varphi \geq 75^\circ$ with $\delta > 1$. Considering that this mixture is dipolar symmetric, the tendency of both species in occupying the same space (not possible due to the miscibility properties) leads to the observed final half-space occupancy for each one of the two components. A critical polarization angle can be defined in this case, which is happening near $\varphi = 75^\circ$. In order to be more precise, we define such critical angle φ_c as being given by the condition that the densities of both species are well defining two maxima, one for each species. This kind of separation of the densities, which we call “angular spatial separation”, occurs for symmetric dipolar mixtures in the immiscible phase. As it will be shown, for the asymmetric cases in their immiscible phase, the spatial separation is radial instead of angular.

The miscibility of the coupled mixture is estimated by using the parameter defined in Eq. (8), which indicates the overlap between the two densities. The results presented in Fig. 2 are shown to be compatible with the ones obtained for non-dipolar systems, given in Ref. [27] (See figure 9 of this reference). from where we can extract that, for $\delta = 0.75$ we have an almost complete miscible system ($\eta = 1$), whereas for $\delta \approx 1.5$ the system becomes almost immiscible ($\eta \approx 0.35$).

In the next, the results given in Fig. 2 are being analyzed by considering the sets with different values of δ . Our analysis is complemented with the next Figs. 3-8. Among the sets with different δ values, the more miscible binary mixture occurs for $\delta = 0.75$, given in Fig. 2(A). With this value for δ and with the rotation frequency $\Omega = 0.6$, we can avoid the collapse of the mixture as the polarization angle is tuned to 90° (more attractive case). This mixture produces squared-lattice structure at $\varphi = 0$. Some distortion are observed near $\varphi = 45^\circ$, but

the square-lattice patterns are sustained up to $\varphi \approx 60^\circ$, as shown in the panels (a_j)-(c_j) of Fig. 2(A). As φ increases, the number of vortices gradually decreases, with a single vortex being shown at $\varphi = 75^\circ$, and disappearing at $\varphi = 90^\circ$, when the rotation $\Omega = 0.6$ is verified not to be enough to form vortices. So, the miscibility of the coupled system becomes almost complete ($\eta \approx 1$) at $\varphi \sim 90^\circ$ due to the dominance of the attractive dipolar forces.

A critical rotation frequency (Ω_c) exists to produce vortices, which can be approximately obtained by using the Feynman rule [37]. According to this rule, derived within a Thomas-Fermi approximation for a single condensate, the total number of vortices (generated by a given rotation frequency) should correspond to $N_v = 2\Omega\langle x^2 \rangle$ (considering our dimensionless units in a quasi-2D spherically symmetric condensate). This rule is only approximately verified in our case when considering a complete repulsive system ($\varphi = 0$), as counting the visible vortices for each component. As we move to attractive systems (higher polarization angles), less number of vortices are shown than the predicted one. However, as already verified for pure dipolar condensates in double-well potential, in Refs. [38, 39], this rule is satisfied when also counting the possible hidden vortices, which can be identified by the phase singularity distributions.

By increasing δ , we show in the set (B) of Fig. 2(B) ($\delta = 1$) the effect of tuning the dipoles, starting with striped vortices ($\varphi = 0^\circ$ and 30°), as verified in the panels (a_j) and (b_j). By increasing φ , striped-shaped vortices are maintained up to $\varphi = 40^\circ$. When the polarization angle $\varphi > 40^\circ$, the number of vortices are not enough to form stripes, with the appearance of double-core vortices. Further increasing of φ up to 90° , only one double-core vortex (for each species $j = 1, 2$) can be observed. The corresponding phase diagrams of the double-core vortices shown in (e_j) of Fig. 2(B) are presented in (a_j) of Fig. 3. As we increase even more δ to 1.1, 1.25, and 1.45, we enter in the immiscible region of the ^{164}Dy - ^{162}Dy binary mixture, which is shown in the sets (C), (D) and (E), respectively, of Fig. 2. In the repulsive cases, shown in the panels (a_j) and (b_j), we observe striped-shaped vortices when $\delta = 1.1$, changing to domain-wall structures for $\delta = 1.25$ and 1.45. For the given δ values, this mixture is space separated radially between $\varphi = 0^\circ$ and some critical orientation angle (φ_c). In this kind of spatial separation, the component with heavy mass (here, component $j = 1$, ^{164}Dy) is located between the lighter one (^{162}Dy , $j = 2$). The lighter one is proliferated around the heavy component. The striped-vortex patterns observed for $\delta = 1.1$ at $\varphi = 0$ continued up to φ close to 60° , as seen in (c_j) of Fig. 2(C). Further, for $\varphi \geq 75^\circ$, we observe an almost complete spatial separation of the mixture.

In order to understand how the spatial separation is occurring in this symmetric dipolar mixture, we consider Fig. 2(C), when $\delta = 1.1$, for polarization angles close to the critical value where an almost complete spatial sep-

aration is observed. For that, we provide in Fig. 4 a set of panels with the densities and the corresponding phase diagrams for the vortex states, by considering the angle φ varying from 67° to 75° . With these panels, we show how we define the critical angles. As we increase φ in this interval, we observe that the initial two maxima verified for $\varphi = 67^\circ$, for each component, reduce to just one maxima when $\varphi = \varphi_c = 75^\circ$, as in the panels (d_j) of Fig. 2(C) (For $\varphi = 74^\circ$ we can still observe two maxima in the densities of one of the components). Interesting enough is the observation of hidden vortices where the component densities are practically absent (at the minimum). These hidden vortices provide enough repulsion for an almost complete spatial separation of the mixture. The densities for the coupled mixture shown in Fig. 2(C), for $\delta = 1.1$, is further analyzed within one-dimensional plots given in four panels of Fig. 5, for $y = 0$, with φ going from 0 to 75° . The almost complete spatial separation of the mixture can be observed at the panel (d) of Fig. 5.

The sets D and E of Fig. 2, respectively for $\delta = 1.25$, and 1.45, are also showing the same behavior of almost complete spatial separation in the attractive part of the dipolar interaction, when the polarization angle $\varphi \geq 75^\circ$. The domain-wall vortex patterns verified when $\varphi = 0$ and 30° start changing when the interaction becomes attractive, at $\varphi = 60^\circ$, until we have the almost complete spatial separation at some critical angle φ_c . Before that, for intermediate angles $\varphi < \varphi_c$, it is possible to observe rotating droplet states, as we can verify particularly in the panels (a_j)-(c_j) of Fig. 2(E). These kind of rotating droplet structures have already been observed in Ref. [40], when considering particular values of δ and rotation angles Ω .

Due to the immiscibility, rotating droplet density peaks are formed near to the surface of the BEC in the first component; being located near the middle of the condensate for the second component. In the structures of the rotating droplets vortex lattice, we observe about vorticity two in the small-sized ones, and about four in the large-sized ones. They are similar as the double-core structures, where rotating droplets in any one of the components are formed by multiple vortices with the same circulation, with vortices in any of those components being surrounded by multiple vortices. The rotating droplet shaped density separations can be observed only within particular parameter regimes of $\delta - \Omega$, when the number of vortices is enough to produce droplets. For the value of $\Omega = 0.6$ we are considering, this condition with rotating droplets being produced is exemplified in the panels (b_j) of Fig. 2(E) (when $\delta = 1.45$ and $\varphi = 30^\circ$). By increasing the polarization angle φ , as exemplified in the panels (c_j) of Fig. 2 (when $\delta = 1.45$), the number of vortices are reduced due to the attractive contributions in the DDI, such that rotating droplets are suppressed.

The effect of rotation, in the case we have an almost complete spatial separation shown for $\delta = 1.1$ and $\varphi = 75^\circ$ in panels (d_j) of Fig. 2(C), can be verified by

switch-off the rotation to $\Omega = 0$. The results, presented in the panels ($a_{j=1,2}$) of Fig. 6, show that in the non-rotating regime the spatial separation is radial, due to the dominant inter-species contact interaction. Such behavior confirms that the observed spatial separation happens in rotating binary mixture due to repulsive forces provided by hidden vortices. In immiscible mixtures of rotating ^{164}Dy - ^{162}Dy condensates, the spatial separation is angular, due to hidden vortices located in both components that are repelling each other. By increasing the polarization angle φ , the DDI becomes more attractive, with a critical angle (φ_c) possible to be identified for an almost complete spatial separation of the mixture.

As the dipole polarizations can change the DDI from repulsive to attractive, it is expected that it will affect the miscibility η of a dipolar coupled system; in a way similar as η being affected by the inter- to intra-species contact interaction δ . In this regard, we should remind from Ref. [28] that, by increasing δ we provide more repulsion between the inter-species, implying that the system becomes less miscible (decreasing η). This effect is clearly shown by the five different curves presented in Fig. 7 when we assume fixed DDI. By increasing the polarization angle φ from 0° , we have the addition of a repulsive DDI effect, which is being reduced till 54.7° , when the DDI is zero. However, when changing φ , all the inter- and intra-species DDI interactions are varying in the same way, keeping the same ratio, such that the main miscibility behavior given by δ is expected to remain.

And, by further increasing φ , for $\varphi > 54.7^\circ$, we have the inter-species repulsive effect due to δ being diminished; at the same time, the attractive intra-species DDI is increasing, which should improve the miscibility of the two species. This behavior is clearly shown for the case that $\delta < 1$ (upper green-line with bullets in the Fig. 7). In this case, we should interpret that the effect of DDI (attractive contribution, in this case) is dominant in comparison with the contact interaction effect. However, for $\delta > 1$, the coupled system is shown to become less miscible when the polarization angle is $\varphi \geq \varphi_c$, besides the attraction provided by the DDI, which is still effective as verified by the shrinking of the radius. As clarified before, for the sizes of the condensates, the intra-species interactions are the relevant observables, such that we conclude that the dipolar ones are dominant in respect to the contact ones. However, for the miscibility, the main role are provided by the inter-species interactions. As the system becomes less miscible for $\varphi \geq \varphi_c$, we conclude that the repulsive inter-species contact interaction are dominant in this region where the DDI is attractive. The combination of both two effects, one due to repulsive contact interactions (reducing the miscibility), with the other due to attractive DDI (reducing the size of the condensates) result in the observed half-space spatial separation of the mixture for larger polarization angles. In summary, one can interpret φ_c as a critical angle at which the system becomes dominated by the DDI, if $\varphi < \varphi_c$; or by the

inter-species contact interactions, if $\varphi > \varphi_c$.

Our results on this study are shown in Fig. 7, where we are verifying that for $\delta = 0.75$ the attractive DDI is dominating, when $\varphi \geq 54.7^\circ$, increasing the miscibility η . With $\delta = 1$, the miscibility of the mixture is weakly affected when tuning the dipoles from repulsive to attractive, but η starts to decrease for large polarization angles, indicating the dominance of contact interactions. Further, for the other three cases considered in Fig. 2 (with $\delta > 1$), we observe the dominant effect of the contact interactions in the immiscibility of the mixture (diminishing η), with φ_c being the critical position where it occurs an almost complete spatial separation of the mixture, with formation of hidden vortices.

In order to estimate the critical angle for the spatial separation, φ_c is obtained as a function of δ in Fig. 8, where we observe that φ_c decreases from 75° to 70° with δ increasing, respectively, from 1.1 to 1.65. By increasing δ , the system becomes less miscible, with the spatial separation being reached for smaller values of φ . Therefore, the complete angular spatial separation is obtained as an accumulative effect of inter-species contact interactions together with repulsive forces due to hidden vortices, in case of rotating coupled condensates. In the non-rotating case, the spatial separation is radial, as shown in Fig. 6.

Resuming our results for the ^{164}Dy - ^{162}Dy binary mixture, we have studied the anisotropic effects due to dipolar interactions by tuning the orientation angle of dipoles from miscible to immiscible cases. The fundamental vortex-lattice structures, which occur for repulsive dipolar interactions ($\varphi < 54.7^\circ$) remain until the attractive dipolar interactions become dominant in respect to the inter- to intra-species contact interactions.

B. The asymmetric-dipolar ^{168}Er - ^{164}Dy binary mixture

In this subsection, we discuss anisotropic effects of dipolar interactions for the asymmetric ^{168}Er - ^{164}Dy mixture. From previous analysis [28], we understand that the vortex-lattice patterns, for repulsive dipolar DDI, mainly feature triangular, squared, and circular vortex lattice structures in this binary mixture. This asymmetric dipolar mixture is less miscible due to the imbalances of dipole moments and atomic masses. It is immiscible even when the inter- to intra-contact interactions are smaller than one ($\delta < 1$), with dominant repulsive inter-species DDI. However, by tuning the dipole polarization angle we can change the DDI to be attractive, which will allow transition between the mixtures. The heavier mass ^{168}Er component, at $\varphi = 0^\circ$, is kept in the center, surrounded by the lighter mass one, ^{164}Dy . By tuning the polarization, increasing φ , the DDI becomes attractive, providing the imbalanced dipolar counterpart. For example, the ^{168}Er has less magnetic moment than the ^{164}Dy , implying that ^{164}Dy will have larger attractive dipolar interaction than the ^{168}Er . This will affect the

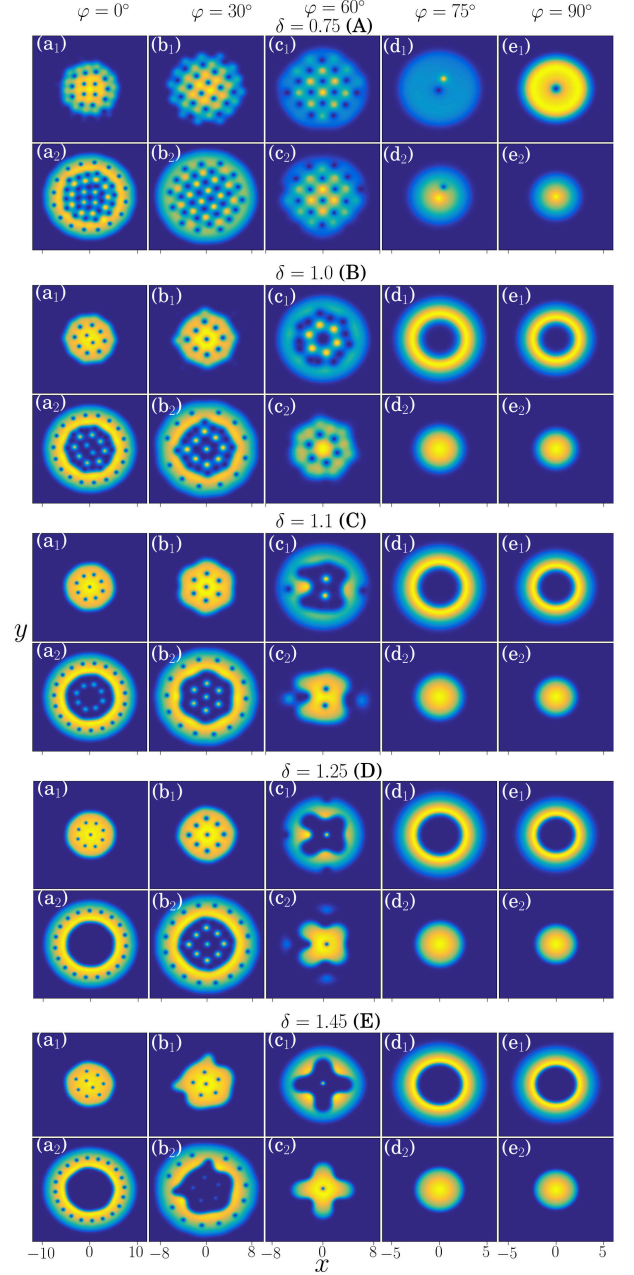


FIG. 9. (Color on line) The 2D densities $|\psi_{j=1,2}|^2$ are shown for the ^{168}Er - ^{164}Dy dipolar mixture ($j = 1$ is the ^{168}Er , with $j = 2$ the ^{164}Dy), by tuning the polarization φ from 0° [(a_j) panels] to 90° [(e_j) panels], with δ varying from 0.75 [set (A)] to 1.45 [set (E)]. As in Fig. 2, all panels have square dimensions, such that only x -labels are indicated, with the corresponding sizes decreasing from left to right. The (x, y) and $|\psi_j|^2$ are dimensionless, with l_\perp being the space unit. The density levels vary from 0 (darker) to a limit ranging $0.01 \sim 0.105$ (lighter), fixed by their respective normalization to one.

corresponding radius of each component in the mixture, with the ^{164}Dy component shrinking more than the ^{168}Er component. The corresponding density distributions, observed for the components in Fig. 9, are clearly indicating this general behavior in all the sets with different values for the contact interactions, by the exchange positions between inner and outer components, as the dipole interactions change from repulsive to attractive.

Here, we should observe that, in the particular case when φ is near 60° , we are close to the polarization “magic angle”, such that the results obtained for the panels (c_j) should approximately correspond to the results presented in the panels (c_j) of Fig. 2. As the mass differences between both dipolar mixtures are quite small, the observed differences in the vortex patterns are mainly due to the fact that with $\varphi = 60^\circ$ we are deviating about 5.3° from φ_M , such that we have some residual dipolar effect due to this deviation. Next, with $\varphi > 54.7^\circ$, we notice some relevant difference between the vortex-patterns obtained in Fig. 9 in relation to the ones shown in Fig. 2 for the symmetric dipolar case. When the attractive dipolar interaction becomes dominant, with the rotation of the mixture the ^{168}Er ($j = 1$) component starts to move from the center to the border, with the ^{164}Dy ($j = 2$) component moving to the center. This behavior can be explained by the fact that the intra-species DDI is less attractive for the species with smaller magnetic moment (in this case, we have $a_{11}^{(d)} < a_{22}^{(d)}$). This interplay between the components can be verified in the panels (c_j) of Fig. 9, when both components are trying to occupy the same localization, with the DDI starting to be attractive. For $\varphi \geq 75^\circ$ [panels (d_j) of Fig.9], we observed that the ^{164}Dy component is already surrounded by the ^{168}Er one, implying in a radial spatial separation. This is more pronounced for the cases that $\delta > 1$, which is expected from previous studies, as a binary mixture becomes less miscible by increasing the repulsive inter-species contact interactions [27, 28].

With Fig. 10 we are presenting our results for the behavior of the miscibility of this asymmetric mixture, ^{168}Er - ^{164}Dy , with respect to the changes in the polarization angle, for each of the sets of δ shown in Fig. 9. In this case, for all the sets we observe a similar behavior of η with respect to φ , with the coupled system becoming more miscible when increasing φ till some critical angle where the miscibility reaches a maximum. The behavior for smaller angles differs from the ones verified in Fig. 7 (where η is not increasing in this interval with $\varphi < 54.7^\circ$). As Er-Dy is a mixture less symmetric than Dy-Dy, for $\varphi = 0^\circ$, it is also less miscible, such that the miscibility is increasing as the DDI becomes less repulsive. For larger polarization angles, we have the combined effect of attractive DDI (reducing the radius and increasing η) together with the repulsive contact interactions till a maximum at some critical φ_c , where there is a balance between the two combined effects. For $\varphi \geq \varphi_c$, the contact interactions start to become dominant in relation to the DDI. Different of the symmetric case observed in Fig. 7,

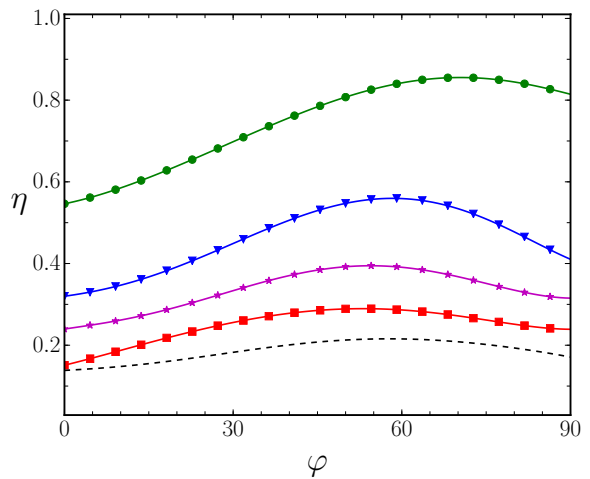


FIG. 10. (Color on line) Miscibility of the dipolar mixture ^{168}Er - ^{164}Dy , defined in Eq. (8) by the parameter η , is shown in respect to the polarization angle φ . For $\delta = 0.75$, we have the green-solid line with circles; for $\delta = 1.0$, the blue-solid line with triangles; for $\delta = 1.1$, the purple-solid line with stars; for $\delta = 1.25$, the red-solid line with squares; and for $\delta = 1.45$ the dashed line.

instead of angular spatial separations, here we are verifying radial spatial separations. As observed in Fig. 10, the critical angles are in a small interval, being $\sim 70^\circ$ for $\delta = 0.75$; $\sim 60^\circ$ for $\delta = 1$; and $\sim 55^\circ$ to $\sim 60^\circ$ for $\delta =$ between 1.1 and 1.45. Next, for $\varphi > \varphi_c$, the system starts to become less miscible with the emergence of the radial spatial separation observed in Fig. 9.

C. The asymmetric-dipolar ^{164}Dy - ^{87}Rb binary mixture

The binary mixture ^{164}Dy - ^{87}Rb is more asymmetric with respect to the dipolar magnetic moments of each component than the other cases that we have considered, with the magnetic moment of ^{87}Rb being almost negligible, such that the effect of the polarization angle is less effective, as due mostly to the ^{164}Dy component. In this case, the rubidium component of the mixture is more concentrated in the center, when considering the region where the DDI is more repulsive (as shown in Fig. 11 for $\varphi = 0$ and 30°), with the dysprosium component distributed within a larger radius. The results are quite similar for the three sets of δ that we are examining. When the DDI changes to an attractive one, as verified for $\varphi \geq 60^\circ$, we observe an interplay between the distributions of the two components, with the radius of the ^{164}Dy (component $j = 1$) being strongly reduced in relation to the radial distribution of the ^{87}Rb ($j = 2$). As in the previous discussed mixture, of erbium and dysprosium, also here the effect is clearly due to the large differences between the magnetic moments of both species: the DDI is more attractive for the species with larger intra-species

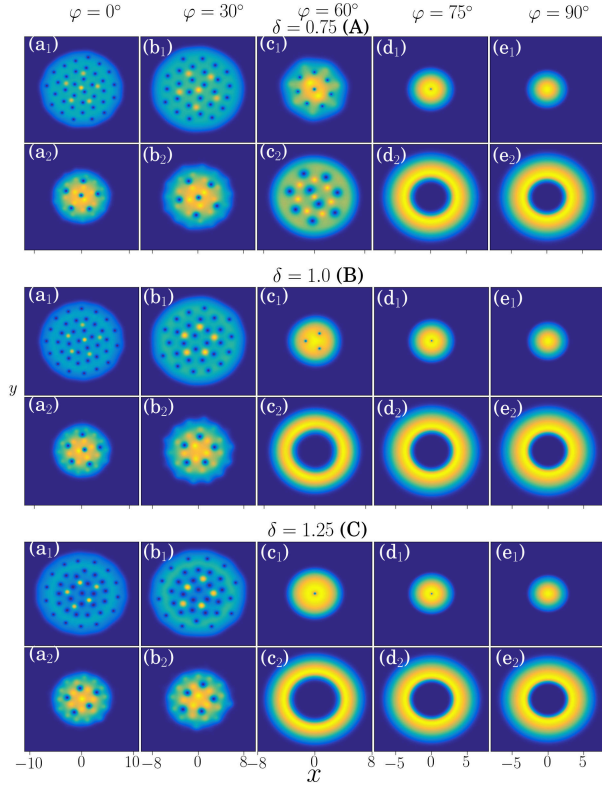


FIG. 11. (Color on line) The 2D densities $|\psi_{j=1,2}|^2$ are shown for the ^{164}Dy - ^{87}Rb dipolar mixture ($j = 1$ is the ^{164}Dy , with $j = 2$ the ^{87}Rb), by tuning the polarization φ from 0 [(a_j) panels] to 90° [(e_j) panels], for $\delta = 0.75$ [set (A)], 1.0 [set (B)] and 1.25 [set (C)]. As in Figs. 2 and 9, all panels have square dimensions, such that only x -labels are indicated, with corresponding sizes decreasing from left to right. The (x, y) and $|\psi_j|^2$ are dimensionless, with $l_\perp = 1\mu\text{m}$ being the space unit. The density levels vary from 0 (darker) to a limit ranging $0.01 \sim 0.08$ (lighter), fixed by their respective normalization to one.

magnetic moment, implying in a smaller radial distribution. In particular, we noticed that this behavior with the corresponding radial spatial separation is happening even for $\delta < 1$, when the DDI becomes attractive. This is reflecting the dominance of the attractive intra-species DDI in relation to the repulsive effects due to the intra-species contact interactions. Apart of that, the radial spatial separation is similar as the one obtained for the ^{168}Er - ^{164}Dy mixture, when the DDI is attractive, with $\delta \geq 1$.

One characteristics of this mixture can be observed when φ is near 60°, which is close to the polarization “magic angle” $\varphi_M = 54.7^\circ$ where the DDI is zero. The results obtained for the panels (c_j) are expected to correspond to the results presented in the panels (c_j) of Fig. 9, if the mass differences were the same. However, in the present case, the mass of the second species, the rubidium, is about half of the dysprosium. So, the results are shown a more clear separation between the species, which can

only be explained by the mass differences, together with the larger difference in the magnetic moments.

IV. SUMMARY AND CONCLUSION

In the present work we are reporting results of a study on anisotropic effects due to dipole-dipole interactions in rotating binary dipolar Bose-Einstein condensates, trapped in a strong pancake-type 2D geometry, obtained by full-numerical solution of the corresponding coupled GP equation. In our approach, the rotating binary mixtures are kept stable, confined by strongly pancake-shaped trap with aspect-ratio $\lambda = 20$ and fixed rotation frequency $0.6\omega_\perp$. Within an investigation that can be generally extended to other kind of dipolar atomic species, we focus our study in binary mixtures having atoms with strong magnetic dipolar properties that are under active investigations in cold-atom laboratories. More specifically, we consider miscible and immiscible regimes of ^{164}Dy - ^{162}Dy , ^{168}Er - ^{164}Dy and ^{164}Dy - ^{87}Rb binary mixtures, which are obtained by changing the inter- to intra-species repulsive two-body contact interactions. The polarization of the dipoles, given by the angle φ , is instrumental in the process of tuning from repulsive to attractive the dipolar interactions for the inter- and intra-atomic species. With the dipoles of the two species polarized in the same direction, perpendicular to the direction of the dipole alignment ($\varphi = 0$), the DDI is repulsive. By tuning the polarization angle φ from zero to 90° the DDI changes from repulsive to fully attractive.

In our study, we first notice that the space distributions of the condensed mixture of each species are mainly affected by the intra-species interactions (repulsive or attractive); with the inter-species interactions being responsible for the vortex-pattern structures, reflecting the miscibility of the mixture (by increasing δ the binary system becomes less miscible). By tuning the polarization angle φ from repulsive to attractive DDI, the vortex-pattern formations obtained with $\varphi = 0$ still survive up to some angle at which the DDI is attractive. Apart from the interesting stable vortex-pattern formations obtained with dipolar-symmetric and dipolar-asymmetric binary mixtures, one of the main outcome of the present study is verified by the almost-complete spatial separation in the two-component densities, which occurs for large polarization angles, when the DDI is attractive. We have verified half-space angular separations of the densities in the case of a dipolar-symmetric mixture, represented by ^{164}Dy - ^{162}Dy , whereas the separations have radial space distribution for the dipolar-asymmetric cases, represented by ^{168}Er - ^{164}Dy and ^{164}Dy - ^{87}Rb . In our study of the miscibility behavior with the polarization angle, we determine the critical polarization angles where the symmetry is broken, leading to the occurrence of an almost-complete space separation of the binary mixtures. As shown, the number of vortices and miscibility of the binary mixtures are significantly affected by the polarization, with the at-

tractive part, obtained by increasing the angle φ , being relevant to reduce the radius of the coupled condensate, merging vortices together and establishing the observed almost-complete space separation.

Another quite relevant result of the present study is the observed effect of the mass-asymmetry in the vortex-pattern structures, which is evidenced in dipolar-symmetric binary mixtures. As shown, the quite small mass-symmetry breaking given by the binary dipolar-symmetric mixture ^{164}Dy - ^{162}Dy is enough to modify significantly the two-species density patterns. This is evidenced by the results with $\delta = 1$. For identical masses, instead of the set of patterns shown in Fig. 2(C), one should verify identical patterns for both species shown at each particular polarization angle. In view of our present conclusion on the mass-symmetry sensibility, when considering a purely mean-field approach for dipolar coupled systems, which could be confirmed experimentally (following Ref. [10]) with binary mixtures having isotopes of the same kind of dipolar atoms, we suggest to

be of high interest further investigations on the role of quantum fluctuations and beyond mean-field properties of coupled dipolar condensates, following Refs. [15, 16]. The physics understanding behind self-bound droplet formation in single and binary dipolar mixtures can be improved by considering effects observed when tuning the dipole-dipole interactions. With dipolar-symmetric mixtures, droplet-like formations are more likely to occur due to the miscibility and competition between repulsive contact and attractive dipolar interactions when tuning the polarization angle.

ACKNOWLEDGEMENTS

RKK acknowledges the financial support from FAPESP of Brazil (Contract number 2014/01668-8). AG and LT thank CAPES, CNPq and FAPESP of Brazil for partial support. LT is also partially supported by INCT-FNA (Proc. No. 464898/2014-5).

-
- [1] A. Griesmaier, J. Werner, S. Hensler, J. Stuhler, and T. Pfau, Bose-Einstein condensation of chromium, *Phys. Rev. Lett.* **94**, 160401 (2005); A. Griesmaier, J. Stuhler, and T. Pfau, Production of a chromium Bose-Einstein condensate, *Appl. Phys. B* **82**, 211 (2006); T. Lahaye, C. Menotti, L. Santos, M. Lewenstein, T. Pfau, The physics of dipolar bosonic quantum gases, *Rep. Prog. Phys.* **72**, 126401 (2009).
 - [2] T. Lahaye, T. Koch, B. Froehlich, M. Fattori, J. Metz, A. Griesmaier, S. Giovanazzi, T. Pfau, Strong dipolar effect in a quantum ferrofluid, *Nature* **448**, 672 (2007).
 - [3] M. Lu, S.H. Youn, and B.L. Lev, Trapping ultracold dysprosium: A highly magnetic gas for dipolar physics, *Phys. Rev. Lett.* **104**, 063001 (2010); M. Lu, N.Q. Burdick, and B.L. Lev, Quantum degenerate dipolar Fermi gas, *Phys. Rev. Lett.* **108**, 215301 (2012).
 - [4] K. Aikawa, A. Frisch, M. Mark, S. Baier, A. Rietzler, R. Grimm, and F. Ferlaino, Bose-Einstein condensation of erbium, *Phys. Rev. Lett.* **108**, 210401 (2012).
 - [5] L. Chomaz, R.M.W. van Bijnen, D. Petter, G. Faraoni, S. Baier, J.H. Becher, M.J. Mark, F. Wächtler, L. Santos, and F. Ferlaino Observation of roton mode population in a dipolar quantum gas, *Nat. Phys.* **14**, 442 (2018).
 - [6] J. Ulitzsch, D. Babik, R. Roell, M. and Weitz, Bose-Einstein condensation of erbium atoms in a quasielectrostatic optical dipole trap, *Phys. Rev. A* **95**, 043614 (2017).
 - [7] J.H. Becher, S. Baier, K. Aikawa, M. Lepers, J.-F. Wyart, O. Dulieu, and F. Ferlaino, Anisotropic polarizability of erbium atoms, *Phys. Rev. A* **97**, 012509 (2018).
 - [8] C. Ravensbergen, V. Corre, E. Soave, M. Kreyer, S. Tzanova, E. Kirilov, and R. Grimm, Accurate determination of the dynamical polarizability of dysprosium, *Phys. Rev. Lett.* **120**, 223001 (2018).
 - [9] V. Veljić, A.R.P. Lima, L. Chomaz, S. Baier, M.J. Mark, F. Ferlaino, A. Pelster, and A. Balaž, Ground state of an ultracold Fermi gas of tilted dipoles in elongated traps, *New J. Phys.* **20**, 093016 (2018).
 - [10] A. Trautmann, P. Ilzhöfer, G. Durastante, C. Politi, M. Sohmen, M.J. Mark, and F. Ferlaino, Dipolar quantum mixtures of erbium and dysprosium atoms, *Phys. Rev. Lett.* **121**, 213601 (2018).
 - [11] P. Ilzhöfer, G. Durastante, A. Patscheider, A. Trautmann, M.J. Mark, and F. Ferlaino, Two-species five-beam magneto-optical trap for erbium and dysprosium, *Phys. Rev. A* **97**, 023633 (2018).
 - [12] E. Lucioni, L. Tanzi, A. Fregosi, J. Catani, S. Gozzini, M. Inguscio, A. Fioretti, C. Gabbanini, and G. Modugno, Dysprosium dipolar Bose-Einstein condensate with broad Feshbach resonances, *Phys. Rev. A* **97**, 060701(R) (2018).
 - [13] Y. Tang, W. Kao, K.-Y. Li, and B.L. Lev, Tuning the dipole-dipole interaction in a quantum gas with a rotating magnetic field, *Phys. Rev. Lett.* **120**, 230401 (2018).
 - [14] Y. Cai, Y. Yuan, M. Rosenkranz, H. Pu, and W. Bao, Vortex patterns and the critical rotational frequency in rotating dipolar Bose-Einstein condensates, *Phys. Rev. A* **98**, 023610 (2018).
 - [15] I. Ferrier-Barbut, H. Kadau, M. Schmitt, M. Wenzel, and T. Pfau, Observation of quantum droplets in a strongly dipolar Bose gas, *Phys. Rev. Lett.* **116**, 215301 (2016); M. Schmitt, M. Wenzel, F. Böttcher, I. Ferrier-Barbut, and T. Pfau, Self-bound droplets of a dilute magnetic quantum liquid, *Nature* **539**, 259-262 (2016).
 - [16] L. Chomaz, S. Baier, D. Petter, M.J. Mark, F. Wächtler, L. Santos, and F. Ferlaino, Quantum-Fluctuation-Driven Crossover from a Dilute Bose-Einstein Condensate to a Macrodroplet in a Dipolar Quantum Fluid, *Phys. Rev. X* **6**, 041039 (2016).
 - [17] V. I. Yukalov, Dipolar and spinor bosonic systems, *Laser Phys.* **28**, 053001 (2018).
 - [18] A.M. Martin, N.G. Marchant, D.H.J. O'Dell, and N.G. Parker, Vortices and vortex lattices in quantum ferrofluids, *J. Phys. Condens. Matter* **29**, 103004 (2017).
 - [19] L. Santos, G.V. Shlyapnikov, and M. Lewenstein, Roton-maxon spectrum and stability of trapped dipolar Bose-Einstein condensates, *Phys. Rev. Lett.* **90**, 250403 (2003).

- [20] D.H.J. O'Dell, S. Giovanazzi, and C. Eberlein, Exact hydrodynamics of a trapped dipolar Bose-Einstein condensate, *Phys. Rev. Lett.* **92**, 250401 (2004).
- [21] S. Yi and L. You, Trapped condensates of atoms with dipole interactions, *Phys. Rev. A* **63**, 053607 (2001); S. Yi and L. You, Expansion of a dipolar condensate, *Phys. Rev. A* **67**, 045601 (2003).
- [22] M. Asad-uz-Zaman and D. Blume, Modification of roton instability due to the presence of a second dipolar Bose-Einstein condensate, *Phys. Rev. A* **83**, 033616 (2011).
- [23] H. Saito, Y. Kawaguchi, and M. Ueda, Ferrofluidity in a two-component dipolar Bose-Einstein condensate, *Phys. Rev. Lett.* **102**, 230403 (2009).
- [24] K.-T. Xi, T. Byrnes, and H. Saito, H. Fingering instabilities and pattern formation in a two-component dipolar Bose-Einstein condensate, *Phys. Rev. A* **97**, 023625 (2018).
- [25] X. Zhang, W. Han, L. Wen, P. Zhang, R.-F. Dong, H. Chang, and S.-G. Zhang, Two-component dipolar Bose-Einstein condensate in concentrically coupled annular traps, *Sci. Rep.* **5**, 8684 (2015).
- [26] R.M. Wilson, C. Ticknor, J.L. Bohn, and E. Timmermans, Roton immiscibility in a two-component dipolar Bose gas, *Phys. Rev. A* **86**, 033606 (2012).
- [27] R.K. Kumar, P. Muruganandam, L. Tomio, and A. Gammal, Miscibility in coupled dipolar and non-dipolar Bose-Einstein condensates, *J. Phys. Commun.* **1**, 035012 (2017).
- [28] R.K. Kumar, L. Tomio, B.A. Malomed, and A. Gammal, Vortex lattices in binary Bose-Einstein condensates with dipole-dipole interactions, *Phys. Rev. A* **96**, 063624 (2017).
- [29] X.F. Zhang, L. Wen, C.-Q. Dai, R.-F. Dong, H.-F. Jiang, H. Chang, and S.-G. Zhang, Exotic vortex lattices in a rotating binary dipolar Bose-Einstein condensate, *Sci. Rep.* **6**, 19380 (2016).
- [30] R.K. Kumar, L. Tomio, and A. Gammal, Vortex patterns in rotating dipolar Bose-Einstein condensate mixtures with squared optical lattices, *J. Phys. B: At. Mol. Opt. Phys.* **52**, 025302 (2019).
- [31] S. Inouye, M.R. Andrews, J. Stenger, H.-J. Miesner, D.M. Stamper-Kurn, and W. Ketterle, Observation of Feshbach resonances in a Bose-Einstein condensate, *Nature* **392**, 151 (1998).
- [32] K. Góral and L. Santos, Ground state and elementary excitations of single and binary Bose-Einstein condensates of trapped dipolar gases, *Phys. Rev. A* **66**, 023613 (2002).
- [33] S. Giovanazzi, A. Görlitz, and T. Pfau, Tuning the dipolar Interaction in quantum gases, *Phys. Rev. Lett.* **89**, 130401 (2002).
- [34] R.K. Kumar, L.E. Young-S, D. Vudragović, A. Balaž, P. Muruganandam, and S.K. Adhikari, Fortran and C programs for the time-dependent dipolar Gross-Pitaevskii equation in an anisotropic trap, *Comput. Phys. Commun.* **195**, 117-128 (2015).
- [35] M. Brtko, A. Gammal, and L. Tomio, Relaxation algorithm to hyperbolic states in Gross-Pitaevskii equation *Phys. Lett. A* **359** 339-344 (2006).
- [36] K. Kasamatsu and M. Tsubota, Vortex sheet in rotating two-component Bose-Einstein condensates *Phys. Rev. A* **79** 023606 (2009).
- [37] A.L. Fetter, Rotating trapped Bose-Einstein condensates, *Rev. Mod. Phys.* **81**, 647-691 (2009).
- [38] S. Subramaniam, Vortex formation and hidden vortices in dipolar Bose-Einstein condensates, *Phys. Lett. A* **381**, 3062-3065 (2017).
- [39] T. Mithum, K. Porsezian, and B. Dey, Pinning of hidden vortices in Bose-Einstein condensates, *Phys. Rev. A* **89**, 053625 (2014).
- [40] K. Kasamatsu, M. Tsubota, and M. Ueda, Vortex phase diagram in rotating two-component Bose-Einstein condensates, *Phys. Rev. Lett.* **91** 150406 (2003).